Dalton Transactions

ROYAL SOCIETY OF CHEMISTRY

PAPER

View Article Online
View Journal | View Issue



Cite this: *Dalton Trans.*, 2025, **54**, 5006

# A blessing and a curse: impact of urea derivatives on the secondary building unit of Ca-MOFs prepared in deep eutectic solvents†‡

Michaël Teixeira, [a] Benoît Louis [b] and Stéphane A. Baudron *[a]

Received 20th November 2024,
Accepted 12th February 2025

DOI: 10.1039/d4dt03254c

rsc.li/dalton

Deep eutectic solvents (DESs) based on a 1 : 2 combination of choline chloride with either urea or e-urea (2-imidazolidinone) have been studied as media for the preparation of Ca(II) metal–organic frameworks (Ca-MOFs). In particular, the impact of the urea derivative on the secondary building unit (SBU) has been investigated by exploring the formation of Ca-MOFs with a series of ten di- and tetra-carboxylic acids, varying in length, steric hindrance and the number and relative orientation of coordinating units. While several of these ligands have, to the best of our knowledge, not been previously reported to form Ca-MOFs, eleven new materials could be prepared and characterized by single-crystal and powder diffraction, elemental and thermogravimetric analyses as well as absorption and emission spectroscopy. The DES incorporating e-urea was found to be especially prone to the formation of crystalline materials. However, a recurrent one-dimensional SBU based on bridging carboxylate moieties and the carbonyl unit of e-urea was observed. Coordination of the solvent molecule is assisted by hydrogen bonding of the NH groups, leading to a strongly stabilizing motif preventing these materials from thermal activation without loss of crystallinity.



## Introduction

Over the past two decades,[1] deep eutectic solvents (DESs) have emerged as an interesting class of media.[2–6] These solvents, formed by mixing two or more compounds in a specific ratio corresponding to the eutectic composition, are characterized by an important freezing point depression (hence the term "deep") in comparison with those of their individual components.[7,8] DESs show appealing properties such as a wide liquid range, non-flammability, low vapor pressure and the ability to dissolve polar species. Furthermore, their chemical and physical properties can be tuned depending on the nature of their components making DESs solvents of choice for a wide array of applications. For example, they are considered as reaction media in organic synthesis,[9–11] for the extraction of diverse compounds,[12] and for drug delivery.[13] In the field of materials science,[14] DESs are being explored as solvents for the ionothermal preparation of metal–organic frameworks (MOFs).[15–18] Indeed, MOFs are commonly synthesized following the solvothermal method in solvents that often feature toxicity and/or flammability[19,20] and for which DESs may represent green alternatives.[21,22] As is usually observed for classical solvents, DES components may be present in the crystalline MOF architectures as ligands of the metal centers or within the pores of the material.[23,24] In particular, MOFs comprising metal–halide bonds normally prone to hydrolysis have been reported using DESs based on a 1 : 2 combination of choline chloride (ChCl) with urea derivatives (Fig. 1).[25,26] This latter type of DES, which has been widely explored for MOF synthesis, has also been shown to allow the formation of porous HKUST-1 and its conversion into a non-porous system.[26] Such urea and e-urea (2-imidazolidinone, ethyleneurea) based DESs (Fig. 1 top) have been employed for the synthesis of Mg-MOF-74 with the nature of the urea derivative and its kinetics of decomposition strongly impacting the crystal morphology and the textural properties of the material.[27] Recently, the use of DES has been extended to another kind of alkaline earth metal MOF with the report of a series of Ca-MOFs based on small aromatic dicarboxylic acids such as terephthalic and isophthalic acids.[28] These three-dimensional architectures rely on a recurrent one-dimensional metallo-organic secondary building unit (SBU) involving bridging carboxylate moieties and e-urea molecules, plugging the channel. Their presence and bridging position prevent activation towards the formation of a porous material without collapse of the crystalline system. In light of the relevance of Ca-MOFs

[a]*Université de Strasbourg, CNRS, CMC UMR 7140, 4 rue Blaise Pascal, F-67000 Strasbourg, France. E-mail: sbaudron@unistra.fr*
[b]*Université de Strasbourg, CNRS, ICPEES UMR 7515, 25 rue Becquerel, F-67087 Strasbourg, France*

† Dedicated to Prof. Marius Andruh on the occasion of his 70th birthday.

‡ Electronic supplementary information (ESI) available: Powder X-ray diffraction patterns, thermogravimetric analysis results, and infra-red and diffuse reflectance spectra of Ca-MOFs **1–11**. CCDC 2403800–2403810. For ESI and crystallographic data in CIF or other electronic format see DOI: **https://doi.org/10.1039/d4dt03254c**

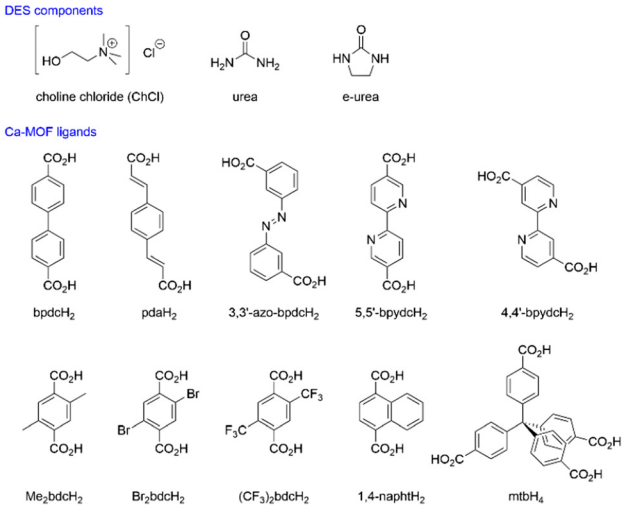


**Fig. 1** Representations of the DES components and the different ligands explored for the preparation of Ca-MOFs in this work.

owing to the lower toxicity of the metal cation and density favourable for gas sorption,[29,30] it appeared to be of interest to further pursue the synthesis of such materials in DES and evaluate the scope of accessible SBUs in these urea-based solvents. To that aim, different parameters may be modified: the size and geometry of the ligand as well as the number of carboxylate units and the nature of the urea derivative comprising the DES. In this work, we have explored these aspects by preparing Ca-MOFs using a series of ten di- and tetra-carboxylic acids in two DESs, ChCl : urea (1 : 2) and ChCl : e-urea (1 : 2) (Fig. 1). Several of these ligands have, to the best of our knowledge, not been previously reported to yield Ca-MOFs. We describe herein the synthesis of these MOFs and their structural characterization by single-crystal and powder X-ray diffraction as well as by thermo-gravimetric analysis and absorption and emission spectroscopy.

## Results and discussion

In addition to the ChCl : e-urea (1 : 2) solvent reported to lead to the formation of Ca-MOFs,[28] the ChCl : urea (1 : 2) analogue, known as reline,[1] has been also investigated to evaluate the impact of a higher number of NH hydrogen bond donor groups as well as the absence of an ethylene group on the formation of the SBU and on the potentially generated porosity. Using these two DESs, a variety of ligands varying in length, steric hindrance and the number and relative orientation of coordinating units have been employed (Fig. 1).

### Impact of the ligand length and orientation/number of carboxylic acid units

To investigate the effect of lengthening dicarboxylic acid ligands, $bpdcH_2$ ([1,1′-biphenyl]-4,4′-dicarboxylic acid), 3,3′-azo-$bdcH_2$ (3,3′-(diazene-1,2-diyl)dibenzoic acid) and $pdaH_2$ (1,4-benzenediacrylic acid) (Fig. 1) were used in ionothermal synthesis in the two aforementioned DESs with $Ca(NO_3)_2{\cdot}4H_2O$ at temperatures varying between 80 and 140 °C. While crystalline materials formed under the conditions explored, four systems afforded crystals large enough for structural determination by single-crystal X-ray diffraction. Thus, three structures were obtained from the e-urea-based DES: [Ca(bpdc)(e-urea)], Ca-MOF **1**, [Ca(3,3′-azo-bdc)(e-urea)], Ca-MOF **2** and [Ca(pda)(e-urea)], Ca-MOF **3**, and one structure from reline [Ca(pda)(urea)], Ca-MOF **4** (Tables 1, 2 and Fig. 2). It is worth noting that Ca-MOFs using $bpdc^{2-}$ have been scarcely described[31] and that **2**, **3** and **4** are, to the best of our knowledge, the first reported Ca-MOFs based on the 3,3′-azo-$bdc^{2-}$ and $pda^{2-}$ ligands. Only Ca-MOFs using olsalazine, the dihydroxyl analogue of 3,3′-azo-$bdcH_2$, have been described.[32] While MOFs **1**–**4** vary in the length of the ligands they are built on, in the orientation of the carboxylate units and the nature of the urea derivative comprising the DES, these four materials all have striking similarities in their crystal structures (Fig. 2). They are built using pillar-like SBUs made of octacoordinated calcium ions linked by the ligand carboxylate moieties coordinated in a chelating bridging $\mu_2$–$\kappa^1$:$\kappa^2$ mode and bridging urea or e-urea molecules coordinated by their oxygen atom. The coordination bond distances are similar for the four MOFs (Table 1). Strikingly, a parallel can be drawn between these structures and the ones obtained in the e-urea-based DES using smaller dicarboxylic ligands such as terephthalic and isophthalic acids.[28]

**Table 1** Selected distances (Å) in the different SBUs and shortest distance between the Ca(II) cations of different SBUs

| | $Ca–O_{carboxylic}$ | $Ca–O_{e\text{-}urea}$ | $Ca–Ca_{SBU}$ | $Ca–Ca_{chains}$ |
|---|---|---|---|---|
| **1** | 2.361(3)–2.525(3) | 2.417(3) | 3.6108(5) | 9.559(1) |
| **2** | 2.3216(12)–2.6235(12) | 2.4466(12) | 3.5808(2) | 10.277(7) |
| **3** | 2.315(3)–2.559(2) | 2.466(2) | 3.5440(4) | 9.893(1) |
| **4** | 2.3308(15)–2.4856(16) | 2.404(2) | 3.4940(3) | 8.287(8) |
| **5** | 2.301(2)–2.342(2) | 2.297(3)–2.351(2) | 5.234(3) | 13.659(1) |
| **6** | 2.2911(15)–2.3599(15) | 2.2835(15) | 5.5041(1) | 11.607(2) |
| **7** | 2.337(3)–2.702(3) | 2.4756(18) | 3.7482(4) | 10.697(8) |
| **8** | 2.3491(13)–2.6641(12) | 2.4378(12)–2.4495(12) | 3.61434(13) | 9.1658(4) |
| **9** | 2.276(6)–2.531(7) | 2.378(6)–2.578(1) | 3.662(2) | 10.130(1) |
| **10** | 2.321(3)–2.561(3) | 2.449(3)–2.488(3) | 3.8599(5) | 9.001(2) |
| **11** | 2.331(5)–2.505(4) | 2.322(5) | 3.8059(11) | 7.856(2) |

**Table 2** Crystallographic data for Ca-MOFs **1–6**

| | **1** | **2** | **3** | **4** | **5** | **6** |
|---|---|---|---|---|---|---|
| Formula | $C_{17}H_{14}CaN_2O_5$ | $C_{17}H_{14}CaN_4O_5$ | $C_{15}H_{14}CaN_2O_5$ | $C_{13}H_{12}CaN_2O_5$ | $C_{18}H_{18}CaN_6O_6$ | $C_{18}H_{18}CaN_6O_6$ |
| FW | 366.38 | 394.40 | 342.36 | 316.33 | 454.46 | 454.46 |
| Crystal system | Orthorhombic | Monoclinic | Orthorhombic | Orthorhombic | Monoclinic | Triclinic |
| Space group | $P2_12_12_1$ | $P2_1/c$ | $P2_12_12_1$ | *Pnma* | $C2/c$ | $P\bar{1}$ |
| $a$/Å | 6.9289(5) | 10.2770(5) | 6.7548(3) | 6.7013(3) | 18.320(4) | 5.5041(7) |
| $b$/Å | 9.9247(6) | 6.8600(3) | 10.3671(7) | 24.4469(8) | 10.321(2) | 8.0865(10) |
| $c$/Å | 25.2185(15) | 25.2747(11) | 22.5867(12) | 8.5707(3) | 21.059(4) | 11.6070(5) |
| $\alpha$/° | | | | | | 120.901(6) |
| $\beta$/° | | 96.901(2) | | | 92.454(14) | 95.514(6) |
| $\gamma$/° | | | | | | 104.903(6) |
| $V$/Å$^3$ | 1734.21(19) | 1768.96(14) | 1581.69(15) | 1404.10(9) | 3978.1(14) | 480.13(11) |
| $Z$ | 4 | 4 | 4 | 4 | 8 | 1 |
| $\lambda$/Å | 0.71073 | 0.71073 | 0.71073 | 0.71073 | 0.71073 | 1.54178 |
| $T$/K | 173(2) | 173(2) | 173(2) | 173(2) | 173(2) | 120(2) |
| $\mu$/mm$^{-1}$ | 0.391 | 0.392 | 0.423 | 0.470 | 0.366 | 3.289 |
| Refls. coll. | 19 870 | 50 732 | 17 081 | 20 423 | 28 648 | 11 096 |
| Ind. refls. ($R_{int}$) | 5081 (0.0990) | 5198 (0.0702) | 4659 (0.0819) | 1652 (0.0818) | 4738 (0.1089) | 1677 (0.0411) |
| $R_1$ ($I > 2\sigma(I)$)[a] | 0.0548 | 0.0438 | 0.0499 | 0.0431 | 0.0549 | 0.0378 |
| w$R_2$ ($I > 2\sigma(I)$)[a] | 0.1006 | 0.0871 | 0.1027 | 0.0898 | 0.1252 | 0.1066 |
| $R_1$ (all data)[a] | 0.0929 | 0.0765 | 0.0754 | 0.0577 | 0.1117 | 0.0396 |
| w$R_2$ (all data)[a] | 0.1153 | 0.0976 | 0.1145 | 0.0954 | 0.1511 | 0.1080 |
| GOF | 1.014 | 1.036 | 1.030 | 1.124 | 1.012 | 1.168 |

[a] $R_1 = \sum||F_o| - |F_c||/\sum|F_o|$; w$R_2 = [\sum w(F_o^2 - F_c^2)^2/\sum wF_o^4]^{1/2}$.

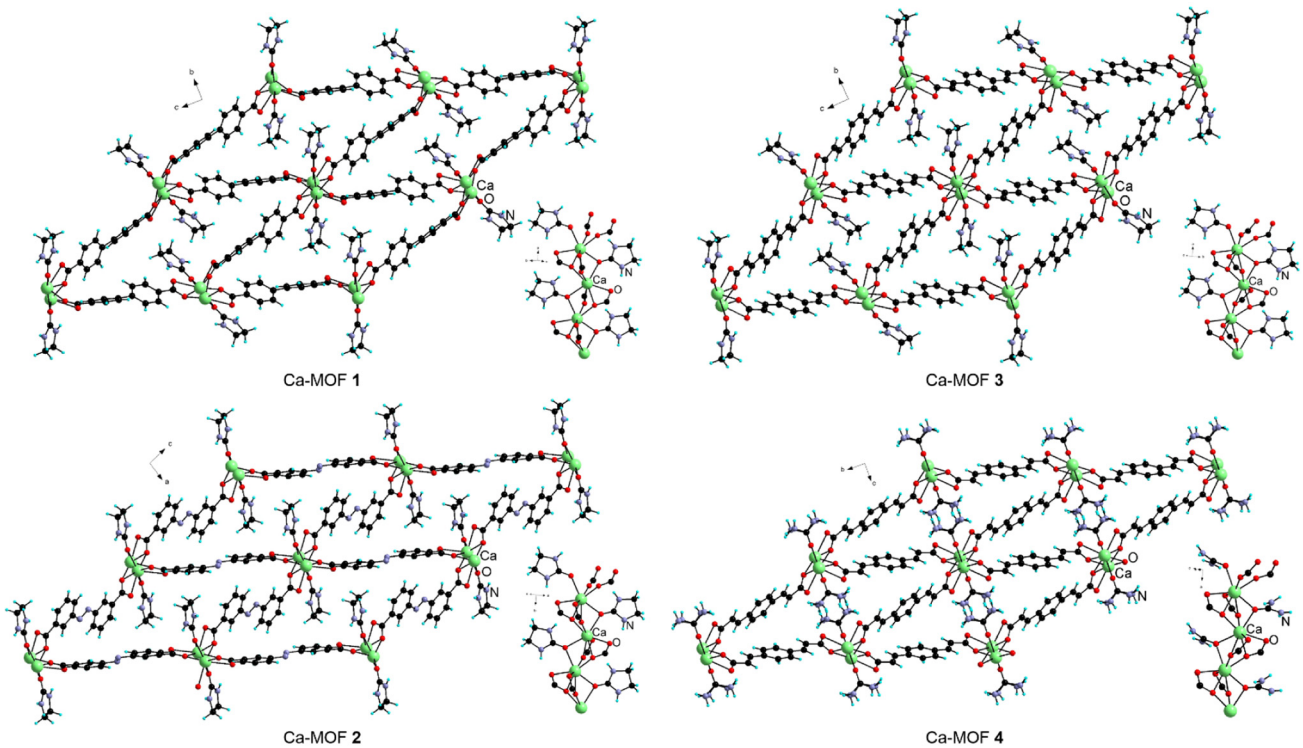


**Fig. 2** The crystal structures of Ca-MOFs **1–4** and their secondary building units.

While the SBU remains the same, the different relative orientations of the carboxylate moieties within the ligand have an effect on the dimensions (ESI Table 3‡) and shape of the channels. In spite of these variations, the pores remain occupied by the coordinated e-urea or urea molecule. In this respect, it is of particular interest to compare Ca-MOFs **3** and **4**, as they are both based on the pda$^{2-}$ ligand but have been obtained from different DESs with the nature of the urea derivative impacting the size and shape of the channels formed. This results not only from the different volumes of

 

these species but also from the different sets of hydrogen bonds (ESI Fig. 36 and Table 1‡). Indeed, while e-urea molecules interact with the carboxylates from their own pillar, urea molecules interact primarily with the adjacent pillar owing to the presence of additional NH groups. This leads to the compression of the channel in the latter case (Fig. 2) as shown by the shorter distance between the SBUs in diagonal positions (Tables 1 and ESI3‡). Interestingly, the SBU and dimensionality of the MOF are modified when using 2,2′-bipyridine-based ligands, analogues of $bpdcH_2$ (Fig. 1). Ca-MOFs **5**, [Ca(5,5′-bpydc)(e-urea)$_2$], and **6**, [Ca(4,4′-bpydc)(e-urea)$_2$], were obtained upon reacting $Ca(NO_3)_2{\cdot}4H_2O$ in ChCl : e-urea (1 : 2) with 2,2′-bipyridine-5,5′-dicarboxylic acid, 5,5′-$bpydcH_2$, 2,2′-bipyridine-4,4′-dicarboxylic acid, and 4,4′-$bpydcH_2$, respectively. Both compounds are two-dimensional networks (Fig. 3) with a one-dimensional SBU comprising a hexa-coordinated Ca(II) center with bridging carboxylates and terminal carbonyl groups of two e-urea molecules. While the latter are *cis* in **5**, they are in a *trans* arrangement in **6**. As the carboxylate groups are solely in a bidentate bridging mode, the distances between the Ca(II) centers within the SBU are longer in **5** and **6** compared with those in **1–4** (Table 1).

Another difference lies in the hydrogen bonding network (ESI Fig. 36 and Table 1‡). For **5**, the e-urea molecule interacts with a neighbouring carboxylate group and another solvent molecule in a self-complementary motif (ESI Fig. 36‡). For **6**, a combination of hydrogen bonding with carboxylate and the central nitrogen atoms of the 4,4′-$bpydc^{2-}$ ligand is observed (ESI Fig. 36‡). It can be noted that **5** and **6** represent rare examples of Ca-MOFs incorporating these 2,2′-bipyridine ligands featuring an uncoordinated diimine unit.[33] In other MOFs, this binding moiety is coordinated either to the Ca cation[34] or another metal center leading to heterometallic systems.[35,36]

Given that the relative orientation of the carboxylate moieties in **5** impacts the SBU, the use of 4,4′,4″,4‴-methanetetrayltetrabenzoic acid, $mtbH_4$, has been investigated, because this tetrahedral ligand has been recently shown to lead to the formation of microporous Ca-MOFs with interesting sorption properties by solvothermal synthesis in DMF.[37,38] Heating a 1 : 2 mixture of this ligand with $Ca(NO_3)_2{\cdot}4H_2O$ in ChCl : e-urea (1 : 2) at 120 °C for 14 days led to crystals of [$Ca_2$(mtb)(e-urea)$_2$], Ca-MOF **7**. This three-dimensional MOF is constructed by bridging *via* the $mtb^{4-}$ ligand of a one-dimensional SBU, analogous to the ones observed in **1–4** (Fig. 4 and Table 1). Therefore, even with a tetrahedral tetraanionic ligand, a similar type of SBU is observed assisted by hydrogen bonding between the e-urea NH groups and the coordinated carboxylate units (ESI Fig. 36 and Table 1‡). This last observation led to the question of the potential impact of the relative steric hindrance around this binding unit and how it would impact the SBU and the hydrogen bonding network.

## Impact of ligand functionalization

It is worth noting that the 2,5-dihydroxyterephthalate ($dobdcH_2^{2-}$) ligand has been reported to lead to Ca-MOFs in DESs.[28] While these materials were shown to be water-sensitive, they feature a SBU with a terminal rather than bridging e-urea molecules. In this context, a series of functionalized $bdcH_2$ derivatives were explored herein (Fig. 1). Functionalization was expected to modify the steric hindrance around the carboxylate moiety and hence to alter the coordination motif and the hydrogen bonding network. Such a strategy is reminiscent of the approach followed for the functionalization of flexible MOFs such as MIL-53(Fe) MOFs, for example, to tune their structure and gas sorption properties.[39] To that aim, three di-functionalized $bdcH_2$ ligands were first explored: 2,5-dimethylterephthalic acid, $Me_2bdcH_2$, 2,5-bis(trifluoro-

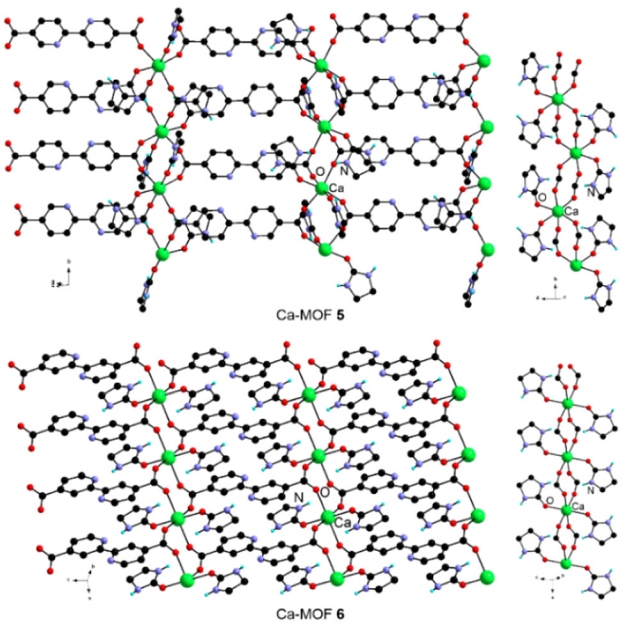


**Fig. 3** The two-dimensional networks in 2,2′-bipyridine based Ca-MOFs **5** and **6** and their secondary building units.

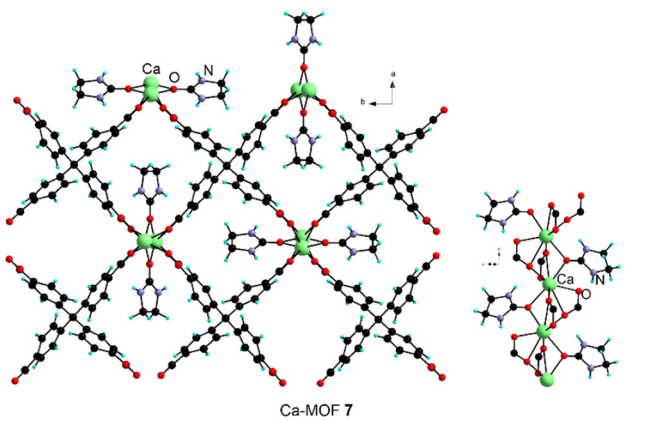


**Fig. 4** View along the *c* axis of the crystal structure of Ca-MOF **7**, left, and of the SBU, right. Only one position of the disordered phenyl rings has been presented for clarity.

methyl)terephthalic acid, $(CF_3)_2bdcH_2$, and 2,5-dibromoterephthalic acid, $Br_2bdcH_2$ (Fig. 1). It can be noted that, to the best of our knowledge, Ca-MOFs have been reported only with $Br_2bdcH_2$,[40] while the former two ligands have not been described to form such Ca-based materials. Once again, upon heating a mixture of the respective ligands and $Ca(NO_3)_2{\cdot}4H_2O$ in ChCl : e-urea (1 : 2) at 120 °C, [Ca($Me_2$bdc)(e-urea)], Ca-MOF **8**, [Ca($(CF_3)_2$bdc)(e-urea)], Ca-MOF **9**, and [Ca($Br_2$bdc)(e-urea)]$_2$(e-urea), Ca-MOF **10**, could be obtained as characterized by single-crystal X-ray diffraction (Table 3). For these three MOFs, ligand bridging of one-dimensional SBUs leads to the formation of a three-dimensional network with channels occupied by e-urea molecules. In the case of Ca-MOFs **8** and **10** (Fig. 5), the SBU is analogous to what has been observed for the reported parent $bdc^{2-}$-based MOF[28] as well as for **1–4** and **7** (Fig. 2 and 4). For these two MOFs, the ligands are stacked in the same orientation. In contrast, for **9**, the $(CF_3)_2bdc^{2-}$ ligands are stacked in an alternating fashion leading to a different SBU where the bridging e-urea molecules are in a *cis* arrangement (Fig. 5).

Expectedly, functionalization at positions 2 and 5 of the $bdc^{2-}$ ligand leads to modified relative orientation of the carboxylate groups with respect to the central phenyl ring. As shown in Fig. 5, the angle between these two types of moieties is 1.9 and 41.2° for the two crystallographically independent $Me_2bdc^{2-}$ anions respectively in **8**, 44.1 and 61.3° for the two $(CF_3)_2bdc^{2-}$ ligands in **9**, and 31.7 and 69.8° for $Br_2bdc^{2-}$ in **10**. For the latter material, this increased twist leads to the presence of e-urea solvate molecules between the ligand along the *b* axis.

To further explore the impact of the functionalization of the $bdcH_2$ ligand on the SBU, 1,4-naphthalenedicarboxylic acid, 1,4-naph$tH_2$, was considered. This derivative has been shown to allow the formation of Ca-MOFs under solvothermal conditions in DMF/$H_2O$ mixtures.[41,42] The reaction of 1,4-naph$tH_2$ with $Ca(NO_3)_2{\cdot}4H_2O$ in ChCl : e-urea (1 : 2) at 120 °C led to the formation of Ca-MOF **11** formulated [Ca(1,4-napht)(e-urea)] (Fig. 6 and Table 3). Ca-MOF **11** is a three-dimensional material constructed by bridging of a one-dimensional SBU. The latter differs from the ones observed in **1–10** as it features hepta-coordinated Ca(II) centers bridged by carboxylate moieties and is also bound to a terminal e-urea molecule (Fig. 6). Interestingly, this organization is reminiscent of the arrangement reported for [Ca(1,4-napht)(DMF)].[41,42] The hydrogen bonding network involves the interaction of the e-urea with a neighbouring carboxylate from the SBU and another solvent molecule in a self-complementary arrangement (ESI Fig. 36 and Table 1‡).

It is worth noting that, for the majority of the ligands explored in this study, sizeable crystals could only be obtained from ChCl : e-urea (1 : 2), while the use of reline afforded only microcrystalline powders, with the exception of Ca-MOF **4** (ESI Table 2‡). This difference in behaviour depending on the solvent may be related to their varying properties. While one may invoke the role of viscosity of the solvent, both DESs are fluid at the reaction temperatures (between 120 and 140 °C). In contrast, their varying decomposition kinetics is known to impact MOF formation. It has been documented that reline decomposes faster than DES analogues based on alkylated urea derivatives.[23,27,43] Indeed, a study on the stability of reline has showed that, after 7 hours at 80 °C, the formation of 0.1% of ammonia was detected.[43] In contrast, it has been observed, in the same study, that with the methylated analogue, only traces of amine could be detected under the same conditions.

**Table 3** Crystallographic data for Ca-MOFs **7–11**

| | **7** | **8** | **9** | **10** | **11** |
|---|---|---|---|---|---|
| Formula | $C_{35}H_{28}Ca_2N_4O_{10}$ | $C_{13}H_{14}CaN_2O_5$ | $C_{13}H_8CaF_6N_2O_5$ | $C_{25}H_{22}Br_4Ca_2N_6O_{11}$ | $C_{15}H_{12}CaN_2O_5$ |
| FW | 774.77 | 318.34 | 426.39 | 982.28 | 340.35 |
| Crystal system | Tetragonal | Monoclinic | Orthorhombic | Monoclinic | Monoclinic |
| Space group | $I\bar{4}2d$ | $P2_1/c$ | $Pnn2$ | $C2/c$ | $C2/c$ |
| $a$/Å | 21.8274(9) | 14.8758(3) | 17.0794(14) | 27.005(3) | 29.6335(16) |
| $b$/Å | | 13.2330(2) | 14.0942(13) | 7.5912(9) | 6.6713(3) |
| $c$/Å | 7.3392(4) | 7.07730(10) | 14.5031(11) | 19.392(2) | 19.3696(10) |
| $\alpha$/° | | | | | |
| $\beta$/° | | 95.263(2) | | 124.491(3) | 130.96(3) |
| $\gamma$/° | | | | | |
| $V$/Å$^3$ | 3496.7(3) | 1387.30(4) | 3491.2(5) | 3276.6(6) | 2916.3(3) |
| $Z$ | 4 | 4 | 8 | 4 | 8 |
| $\lambda$/Å | 0.71073 | 0.67199 | 0.71073 | 0.71073 | 1.54178 |
| $T$/K | 173(2) | 100(2) | 173(2) | 120(2) | 120(2) |
| $\mu$/mm$^{-1}$ | 0.389 | 0.476 | 0.448 | 5.293 | 3.984 |
| Refls. coll. | 73 203 | 21 062 | 28 528 | 30 089 | 9480 |
| Ind. refls. ($R_{int}$) | 2583 (0.0824) | 3467 (0.0904) | 8071 (0.1353) | 4812 (0.0973) | 2541 (0.0489) |
| $R_1$ ($I > 2\sigma(I)$)[a] | 0.0439 | 0.0433 | 0.0588 | 0.0530 | 0.0803 |
| w$R_2$ ($I > 2\sigma(I)$)[a] | 0.1020 | 0.1184 | 0.0937 | 0.0894 | 0.2232 |
| $R_1$ (all data)[a] | 0.0598 | 0.0459 | 0.1485 | 0.0973 | 0.0868 |
| w$R_2$ (all data)[a] | 0.1112 | 0.1212 | 0.1199 | 0.1080 | 0.2342 |
| GOF | 1.057 | 0.982 | 0.960 | 1.122 | 1.100 |

[a] $R_1 = \sum||F_o| - |F_c||/\sum|F_o|$; w$R_2 = [\sum w(F_o^2 - F_c^2)^2/\sum wF_o^4]^{1/2}$.

 

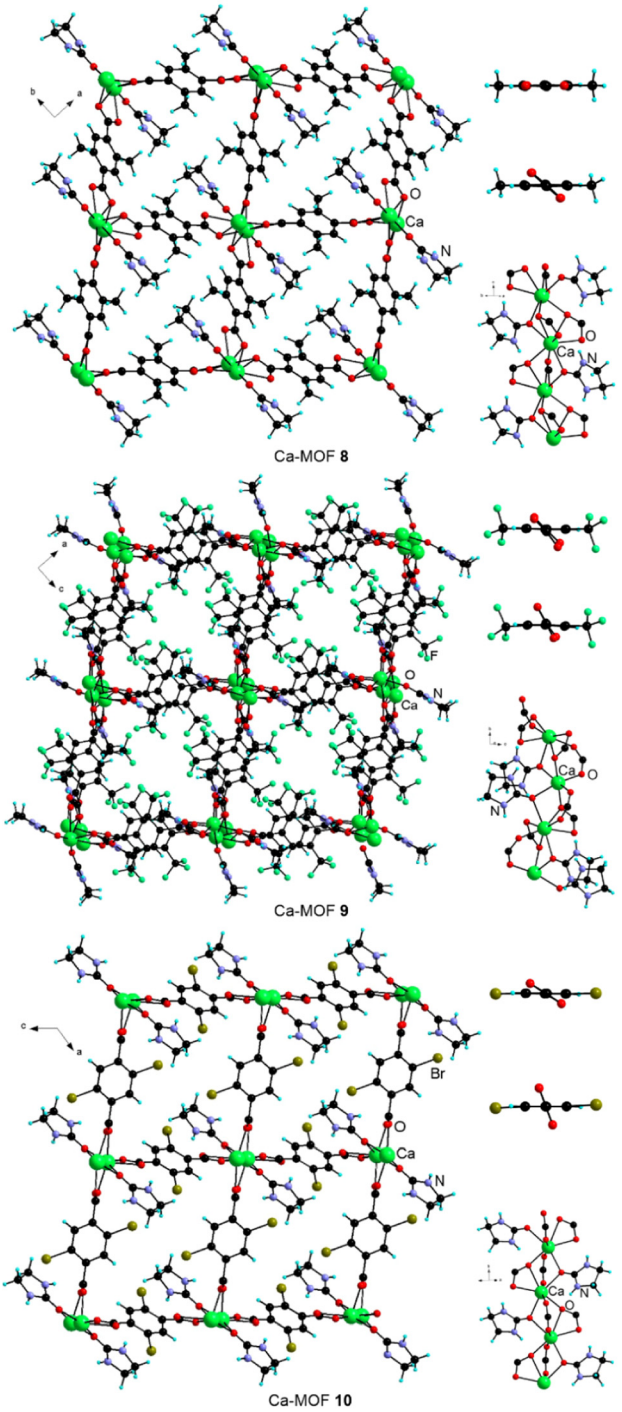


**Fig. 5** The crystal structure of Ca-MOFs **8–10** and of their secondary building units and side view of the ligands highlighting the functionalization-dependent relative orientation of the phenyl and carboxylate moieties. For **10**, the e-urea solvate molecule has been omitted for clarity.

Similarly, a study on the decomposition of the 1 : 2 ChCl : e-urea DES by $^{1}$H NMR spectroscopy confirmed that ethylene diamine is barely visible after heating at 200 °C for 12 h, whereas more extensive degradation was observed after 6 days,

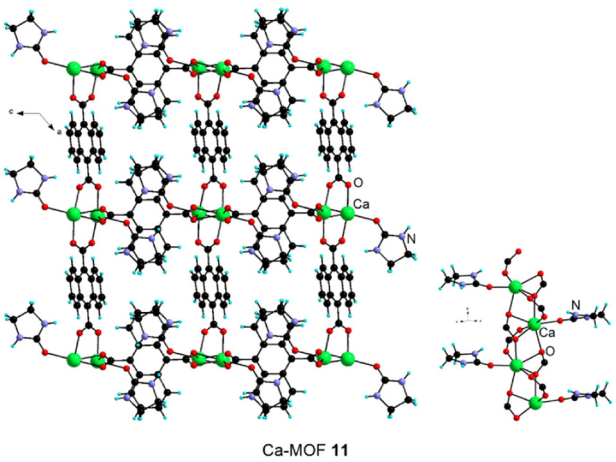


**Fig. 6** The crystal structure of Ca-MOF **11** and its SBU. Note that, owing to symmetry operations, the naphthalene unit appears over two positions.

in particular in the presence of metal salts and ligands necessary for framework formation.[23] Hence, the release of either ammonia or ethylene diamine for the two respective DESs follows varying kinetics leading to different evolution of the basicity of the solution, thereby impacting the deprotonation of the ligand towards the formation of MOFs. This has been thoroughly investigated in the preparation of Mg-MOF-74 with the synthesis in reline providing smaller crystals and more rapidly than for the e-urea based DES.[27] Furthermore, the observed formation of intermediate crystalline phases either involving e-urea or a partially deprotonated ligand prompted longer reaction time and higher heating temperature, for this system (3 days at 140 °C *vs.* 2 days at 120 °C in reline).[27] Based on these previous reports, it can be hypothesized that, in reline, fast release of ammonia already leads to deprotonation of the ligand after a few hours, resulting in faster formation of solid materials, hence the isolation of microcrystalline powders. Working under more dilute conditions in reline has unfortunately not yet led to an increase in crystal size sufficient for singe-crystal X-ray diffraction experiments. In contrast, in 1 : 2 ChCl : e-urea, reactions were allowed to proceed for several weeks to ensure the highest crystal quality, to prevent the potential presence of intermediate compounds and owing to the limited solubility of some of the ligands. Shortening of the reaction time in this context was not further investigated.

The eleven MOFs were characterized by X-ray powder diffraction. **1–4**, **8–9** and **11** were found to show a good match between the pattern calculated from single-crystal data and the experimental one (ESI Fig. 1–9‡) suggesting the presence of a single crystalline phase. In the case of **6**, additional peaks and a slight shift in the position of some of the peaks compared with the calculated diagram (ESI Fig. 5‡) suggest that the isolated phase characterized by single-crystal X-ray diffraction may not be the sole product and that another structurally related MOF, which could not be further analyzed, also forms.

A few very small additional peaks corresponding to an unidentified additional compound were observed for **7**. No satisfactory data could be obtained for **5** and **10**. For **5**, this may be related to the remaining starting ligand (*vide infra*), while, for **10**, it is consistent with the fact that this Ca-MOF was found to be sensitive to water from the atmosphere. This sensitivity may be related to the presence of the bromo substituents lowering the p$K_a$ of the carboxylic acid, hence weakening the coordination bond. Furthermore, while good agreement between the calculated and experimental diffraction patterns for **2** is observed (ESI Fig. 2‡), the peaks are slightly broadened, also suggesting sensitivity to air and/or humidity leading to fragmentation of the crystallites and reduction of the scattering volume, as reported for other Ca-MOFs.[28] It can be noted that, in contrast, **1**, **3–9** and **11** are all stable in air. However, all these materials were found to quickly dissolve in water, even **9** incorporating hydrophobic $CF_3$ groups. While this water solubility may be a problem for gas sorption, one may consider these materials for the release of either urea or e-urea in agricultural applications.[44,45]

The compounds were also characterized by elemental analysis confirming their chemical purity except for **1**, **5** and **6**. Characterization by infra-red spectroscopy provided further insights (ESI Fig. 26–35‡). In the case of **1**, the spectra of the MOF and the starting ligand (ESI Fig. 26‡) show numerous common absorption bands suggesting the presence of the remaining insoluble ligand, consistent with the elemental analysis result. For **5** and **6**, however, the infra-red spectra do not show the remaining starting ligand, and therefore, consistent with the X-ray powder diffraction results (*vide supra*), the formation of other crystalline materials may be at stake.

The MOFs presented in this study feature urea derivatives plugging the channels, hence blocking potential porosity as demonstrated by the small pore limiting diameter (ESI Table 3‡). This diameter is naturally substantially increased, leading to potential porosity, following theoretical removal of coordinated solvent molecules, considering a retention of the framework structure (ESI Table 3‡). This prompted the study of the potential activation of these MOFs.[46] Thermo-gravimetric analysis of the materials was thus performed. A weight loss at temperatures ranging from 200 to 400 °C depending on the ligand is observed, corresponding to the decomposition of the materials, as it accounts for more than the weight of the incorporated e-urea (ESI Fig. 10–17‡). This phenomenon unfortunately prevented the investigation of thermal activation[46] of the MOFs towards the removal of coordinated solvent molecules while maintaining the structural integrity of the frameworks for the study of their textural properties. While this observation is expected for the materials based on an SBU featuring a bridging e-urea molecule, this is more surprising for the 3-D MOF **11** with terminal e-urea. Our attempts at activating this latter MOF either thermally or by solvent exchange led to a loss of crystallinity, limiting further study of its porosity.

The diffuse reflectance spectra of Ca-MOFs **1–11** feature a broad absorption band for the different compounds (ESI Fig. 18–25‡). Investigation of their luminescence indicated no detectable emission for **1–10**, whereas emission at 396 nm upon excitation at 320 nm was observed for Ca-MOF **11** (Fig. 7). This represents a significant blue shift in comparison with the emission maximum at 496 nm for the free 1,4-naphth$H_2$ ligand (Fig. 7) and is consistent with what has been reported for [Ca(1,4-napht)(DMF)].[41]

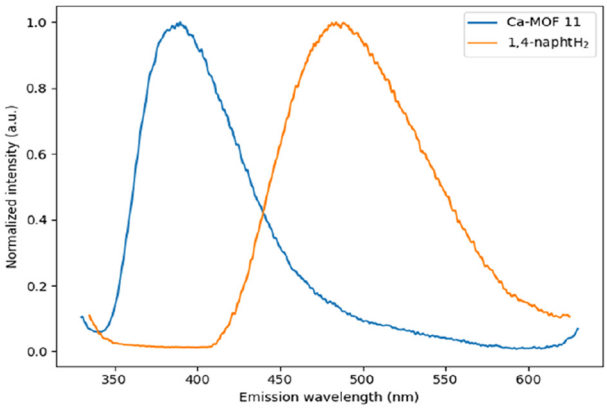


**Fig. 7** Solid state emission spectra of free 1,4-naphth$H_2$ (orange line) and Ca-MOF **11** (blue line) upon excitation at 320 nm at room temperature.

## Conclusions

Deep eutectic solvents based on the 1 : 2 combination of ChCl with either urea or e-urea have been shown to be efficient media for the formation of Ca-MOFs with a series of ten different ligands, some of which had not been reported so far to yield Ca-MOFs. In particular, the system incorporating e-urea has demonstrated its ability to form materials featuring a SBU with bridging solvent molecules, as observed for the majority of MOFs prepared herein, **1–4**, **7–8** and **10**. While the recurrence of this SBU is interesting, the robustness of this motif impairs the activation of the materials towards investigation/exploitation of their porosity, representing both a blessing and a curse on a search for new porous systems. Lengthening of the ligand and modification of the number and orientation of binding units and of the steric hindrance have not led to a substantial alteration of the SBU with the exception of the 4,4′-bipyridine and 1,4-naphthalene based ligands affording two-dimensional **5** and **6** and three-dimensional **11** showing terminal e-urea molecules. However, as demonstrated by thermogravimetric analysis and our unsuccessful attempts to activate **11**, the solvent could not be removed to take full benefit from the potential porosity of this material. One key aspect probably resides in the combination of the coordination of the carbonyl group and hydrogen bonding of the NH moieties as a structuring motif. It is worth noting that such a phenomenon has not been reported in the synthesis of Mg-MOF-74, where the urea derivatives impact the morphology and textural properties but not the structure with

the absence of these species in the SBU.[27] This probably calls for an investigation with other alkaline earth metal cations such as Mg(II), Sr(II) or Ba(II). The role of ChCl in the formation of the MOFs also requires further investigation. While it allows the formation of the deep eutectic solvent, hence lowering the melting point to render the urea species amenable for their use as solvents, it is not present in the structures described herein. Therefore, it would be of interest to explore the urothermal method[47] consisting in using a pure urea derivative as reaction medium for the formation of Ca-MOFs, for example alkylated urea derivatives. Alternatively, synthesis in DESs not incorporating urea species altogether could be considered.[48] These studies are currently under way and will be published in due course.

## Experimental section

### Synthesis

**DES preparation.** All DESs[1,23] were prepared before each synthesis by heating the mixture under stirring in a round-bottom flask, until a homogeneous liquid phase was formed. The following mixtures and temperatures were used:

ChCl : urea 1 : 2 (reline) at 50 °C.

ChCl : e-urea 1 : 2 at 90 °C.

### General MOF synthesis procedure

The reagents were added to a vial before the addition of the DES. While reline is a liquid at room temperature (m.p. = 12 °C),[1] the 1 : 2 ChCl : e-urea DES is solid (m.p. = 70 °C).[23] The 1 : 2 ChCl : e-urea DES, that is therefore solid at room temperature, was manipulated while hot using preheated syringes. Upon addition of the DES, the vial was heated in a dry bath. The formation of crystals could be observed after a few days and the reaction was pursued to ensure maximum crystallinity and purity of the MOFs. After completion of the reaction, ethanol was added quickly, before letting the vial cool down, to prevent solidification of the DES and to allow recovery of the MOF. The resulting mixture was then filtered and washed multiple times with ethanol to remove any traces of the DES. The remaining solid was air-dried.

**Ca-MOF 1 ([Ca(bpdc)(e-urea)]).** Biphenyl-4,4′-dicarboxylic acid (0.194 g, 0.8 mmol) and $Ca(NO_3)_2{\cdot}4H_2O$ (0.378 g, 1.6 mmol) were added to a 20 mL vial before the addition of freshly prepared ChCl : e-urea DES (1 : 2, 10 mL). The vial was then heated at 120 °C for 14 days. The reaction was performed according to the general procedure. The product could not be purified, owing to the presence of the remaining insoluble ligand, as confirmed by infra-red spectroscopy.

**Ca-MOF 2 ([Ca(3,3′-azo-bdc)(e-urea)]).** Azobenzene-3,3′-dicarboxylic acid (0.216 g, 0.8 mmol) and $Ca(NO_3)_2{\cdot}4H_2O$ (0.378 g, 1.6 mmol) were added to a 20 mL vial before the addition of freshly prepared ChCl : e-urea DES (1 : 2, 10 mL). The vial was then heated at 120 °C for 17 days. The reaction was performed according to the general procedure (0.274 g, 86.8%). Elemental analysis (CHN) of $C_{17}H_{14}CaN_4O_5$; calculated: C, 51.77; H, 3.58; N, 14.21; found: C, 51.42; H, 3.59; N, 14.22.

**Ca-MOF 3 ([Ca(pda)(e-urea)]).** 1,4-Phenylenediacrylic acid (0.044 g, 0.2 mmol) and $Ca(NO_3)_2{\cdot}4H_2O$ (0.094 g, 0.4 mmol) were added to a 8 mL vial before the addition of freshly prepared ChCl : e-urea DES (1 : 2, 2.5 mL). The vial was then heated at 140 °C for 14 days. The reaction was performed according to the general procedure (0.0375 g, 54.8%). Elemental analysis (CHN) of $C_{15}H_{14}CaN_2O_5$; calculated: C, 52.62; H, 4.12; N, 8.18; found: C, 51.82; H, 4.18; N, 8.37.

**Ca-MOF 4 ([Ca(pda)(urea)]).** 1,4-Phenylenediacrylic acid (0.174 g, 0.8 mmol) and $Ca(NO_3)_2{\cdot}4H_2O$ (0.378 g, 1.6 mmol) were added to a 20 mL vial before the addition of freshly prepared ChCl : urea DES (1 : 2, 10 mL). The vial was then heated at 120 °C for 14 days. The reaction was performed according to the general procedure (0.219 g, 86.6%). Elemental analysis (CHN) for $C_{13}H_{12}CaN_2O_5$; calculated: C, 49.36; H, 3.82; N, 8.86; found: C, 48.32; H, 3.91; N, 8.83.

**Ca-MOF 5 ([Ca(5,5′-bpydc)(e-urea)$_2$]).** 2,2′-Bipyridine-5,5′-dicarboxylic acid (0.049 g, 0.2 mmol) and $Ca(NO_3)_2{\cdot}4H_2O$ (0.094 g, 0.4 mmol) were added to a 20 mL vial before the addition of freshly prepared ChCl : e-urea DES (1 : 2, 10 mL). The vial was then heated at 120 °C for 7 weeks. The reaction was performed according to the general procedure. No satisfactory elemental analysis could be performed owing to the formation of several crystalline phases as confirmed by powder X-ray diffraction.

**Ca-MOF 6 ([Ca(4,4′-bpydc)(e-urea)$_2$]).** 2,2′-Bipyridine-4,4′-dicarboxylic acid (0.049 g, 0.2 mmol) and $Ca(NO_3)_2{\cdot}4H_2O$ (0.094 g, 0.4 mmol) were added to a 20 mL vial before the addition of freshly prepared ChCl : e-urea DES (1 : 2, 10 mL). The vial was then heated at 120 °C for 7 weeks. The reaction was performed according to the general procedure. No satisfactory elemental analysis could be performed owing to the formation of several crystalline phases as confirmed by powder X-ray diffraction.

**Ca-MOF 7 ([Ca$_2$(mtb)(e-urea)$_2$]).** 4,4′,4″,4‴-Methanetetrayltetrabenzoic acid (0.040 g, 0.08 mmol) and $Ca(NO_3)_2{\cdot}4H_2O$ (0.0378 g, 0.16 mmol) were added to an 8 mL vial before the addition of freshly prepared ChCl : e-urea DES (1 : 2, 2.5 mL). The vial was then heated at 120 °C for 14 days. The reaction was performed according to the general procedure (0.0203 g, 34.1%). Elemental analysis (CHN) of $C_{35}H_{28}Ca_2N_4O_{10}$; calculated: C, 56.44; H, 3.79; N, 7.52; found: C, 55.41; H, 4.17; N, 8.34.

**Ca-MOF 8 ([Ca(Me$_2$bdc)(e-urea)]).** 2,5-Dimethylterephthalic acid (0.019 g, 0.1 mmol) and $Ca(NO_3)_2{\cdot}4H_2O$ (0.047 g, 0.2 mmol) were added to a 20 mL vial before the addition of freshly prepared ChCl : e-urea DES (1 : 2, 10 mL). The vial was then heated at 120 °C for 21 days. The reaction was performed according to the general procedure (0.0153 g, 48.1%). Elemental analysis (CHN) of $C_{13}H_{14}CaN_2O_5$; calculated: C, 49.05; H, 4.43; N, 8.80; found: C, 47.81; H, 4.51; N, 8.76.

**Ca-MOF 9 ([Ca((CF$_3$)$_2$bdc)(e-urea)]).** 2,5-Bis(trifluoromethyl) terephthalic acid (0.030 g, 0.1 mmol) and $Ca(NO_3)_2{\cdot}4H_2O$ (0.047 g, 0.2 mmol) were added to an 8 mL vial before the

addition of freshly prepared ChCl : e-urea DES (1 : 2, 2.5 mL). The vial was then heated at 120 °C for 28 days. The reaction was performed according to the general procedure (0.0170 g, 39.9%). Elemental analysis (CHN) for $C_{13}H_8CaF_6N_2O_5$; calculated: C, 36.63; H, 1.89; N, 6.57; found: C, 36.36; H, 2.08; N, 6.60.

**Ca-MOF 10 ([$Ca_2$($Br_2$bdc)$_2$(e-urea)$_2$](e-urea)).** 2,5-Dibromoterephthalic acid (0.032 g, 0.1 mmol) and $Ca(NO_3)_2{\cdot}4H_2O$ (0.047 g, 0.2 mmol) were added to an 8 mL vial before the addition of freshly prepared ChCl : e-urea DES (1 : 2, 2.5 mL). The vial was then heated at 120 °C for 2 months. The reaction was performed according to the general procedure (0.0215 g, 52.3%). Elemental analysis (CHN) of $C_{25}H_{22}Br_2Ca_2N_6O_{11}$; calculated: C, 30.57; H, 2.26; N, 8.56; found: C, 30.33; H, 2.83; N, 8.89.

**Ca-MOF 11 ([Ca(napht)(e-urea)]).** 1,4-Naphthalenedicarboxylic acid (0.173 g, 0.8 mmol) and $Ca(NO_3)_2{\cdot}4H_2O$ (0.189 g, 0.8 mmol) were added to a 20 mL vial before the addition of freshly prepared ChCl : e-urea DES (1 : 2, 10 mL). The vial was then heated at 120 °C for 28 days. The reaction was performed according to the general procedure (0.163 g, 59.8%). Elemental analysis (CHN) of $C_{15}H_{12}CaN_2O_5$; calculated: C, 52.94; H, 3.55; N, 8.23; found: C, 51.99; H, 3.58; N, 8.79.

### Elemental analysis

Elemental analyses (CHN) were performed at the Service Commun d'Analyses of the University of Strasbourg, in duplicate, employing Thermo Fisher FLASH 2000 equipment, whereas the reported values for CHN were taken as the average of two measurements.

### Thermo-gravimetric analysis

The thermal stability of the samples was determined on a PerkinElmer thermogravimetric analyzer TGA 4000 under a $N_2$ flow of 20 mL $min^{-1}$ and at a heating rate of 5 °C $min^{-1}$ up to 800 °C.

### Optical properties

Diffuse reflectance spectra were collected on a PerkinElmer Lambda 650S UV-vis spectrometer at room temperature. Emission spectra were collected on a PerkinElmer LS55 fluorescence spectrometer at room temperature.

### Infra-red spectroscopy

Infra-red spectra were collected at room temperature on a PerkinElmer FTIR-UATR spectrum two spectrometer by attenuated total reflectance on powders.

### X-ray diffraction

Data for **1–4** and **7** were collected at 173 K on a Bruker SMART CCD diffractometer with Mo-Kα radiation. All structures were solved using SHELXS-97 and refined by full matrix least-squares on $F^2$ using SHELXL-2016 with anisotropic thermal parameters for all non-hydrogen atoms. The hydrogen atoms were introduced at the calculated positions and not refined (riding model). For **7**, a certain degree of disorder has been found and the four phenyl rings of the $mtb^{4-}$ ligands have been modeled accordingly over two positions. Regarding the atoms of the e-urea molecules showing also very anisotropic ellipsoids, attempts at modeling a potential disorder using the PART command or imposing constraints (EADP) did not lead to an improvement of the refinement.

X-ray diffraction data collection for **5** and **9** was carried out on a Bruker APEX II DUO Kappa-CCD diffractometer equipped with an Oxford Cryosystem liquid $N_2$ device, using Mo-Kα radiation ($\lambda$ = 0.71073 Å). The crystal–detector distance was 38 mm. The cell parameters were determined (APEX4 software)[49] from reflections taken from 3 sets of 6 frames at 10 s exposure. The structure was solved using the program SHELXT-2018.[50] The refinement and all further calculations were carried out using SHELXL-2019.[51] The H-atoms were included in calculated positions and treated as riding atoms using SHELXL default parameters. The non-H atoms were refined anisotropically, using weighted full-matrix least-squares on $F^2$. A semi-empirical absorption correction was applied using SADABS in APEX4;[49] transmission factors: $T_{min}/T_{max}$ = 0.7036/0.7456. For **9**, some atoms are highly prolate. As for **7**, similar attempts at addressing this did not lead to an improvement of the refinement and crystals of better quality for better data for structure determination could not be isolated.

X-Ray diffraction data collection for **6**, **10** and **11** was carried out on a Bruker PHOTON-III DUO CPAD diffractometer equipped with an Oxford Cryosystem liquid $N_2$ device, using Mo-Kα radiation ($\lambda$ = 0.71073 Å). The crystal–detector distance was 37 mm. The cell parameters were determined (APEX4 software)[49] from reflections taken from one set of 180 frames, each at 1 s exposure. The structures were solved using the program SHELXT-2018.[50] The refinement and all further calculations were carried out using SHELXL-2018.[51] The H-atoms were included in calculated positions and treated as riding atoms using SHELXL default parameters. The non-H atoms were refined anisotropically, using weighted full-matrix least-squares on $F^2$. A semi-empirical absorption correction was applied using SADABS in APEX4;[49] transmission factors: $T_{min}/T_{max}$ = 0.6544/0.7458.

The single-crystal X-ray diffraction data acquisition of Ca-MOF **8** was carried out at the CRISTAL beamline (synchrotron SOLEIL, Paris) using the synchrotron radiation source ($\lambda$ = 0.67199 Å). Diffraction intensities were measured using a CCD detector (Atlas detector from Rigaku) mounted on a four-circle MKS-Newport diffractometer. The crystal-to-detector distance was set to 80 mm. The temperature for data collection ($T$ = 100 K) was reached with a gas streamer (Cryo Industries of America). The wavelength was selected with a double crystal monochromator (Si 111 crystals) and sagittal (horizontal) focusing was achieved using a 1D SU-8 compound refractive lens system developed by the Karlsruhe Institute of Technology. The beam attenuation was performed using Al (or Cu) foils of different thicknesses inserted in the incident beam. Data collection strategies, refinement of the unit cell parameters and data reduction were carried out using the CrysAlisPro software package.[52] The refinement and all further calculations were carried out using SHELXL-2018.[51]

 

Powder X-ray diffraction patterns were recorded at 293 K on a Bruker D8 diffractometer using monochromatic Cu-Kα radiation with a scanning range between 3 and 40° using a scan step of 0.0225° $min^{-1}$, with the compound placed on a rotating Si low background sample holder. The calculated diagrams were generated with the Mercury® software based on the single-crystal data collected.

The pore analyzer module of this software was employed for the calculation of the pore limiting and maximum pore diameters.

## Author contributions

Investigation: M. T. and S. A. B.; methodology: M. T. and S. A. B.; writing – original draft: S. A. B.; writing – review & editing: M. T. and B. L.; and funding acquisition: B. L. and S. A. B.

## Data availability

The data supporting this article (powder X-ray diffraction patterns, thermogravimetric analysis results, and infra-red and diffuse reflectance spectra of Ca-MOFs **1–11**) have been included as part of the ESI.‡

Crystallographic data for Ca-MOFs **1–11** have been deposited at the CCDC under 2403800–2403810.‡

## Conflicts of interest

There are no conflicts to declare.

## Acknowledgements

This work has benefited from support provided by the University of Strasbourg Institute of Advanced Study (USIAS), within the French national programme "Investment for the future" (IdEx-Unistra). We also thank the Université de Strasbourg, the C.N.R.S., and the Ministère de l'Enseignement Supérieur, de la Recherche et de l'Innovation (Ph. D. fellowship of Michaël Teixeira) for financial support. We acknowledge SOLEIL for provision of synchrotron radiation facilities and we would like to thank Dr Pierre Fertey for assistance in using beamline CRISTAL (BAG 20231465). We thank Corinne Bailly and Nathalie Gruber (University of Strasbourg) for assistance in the crystal structure determination of **6**, **10–11**.

## References

1 A. P. Abbott, G. Capper, D. L. Davies, R. K. Rasheed and V. Tambyrajah, *Chem. Commun.*, 2003, 70.
2 Q. Zhang, K. de Oliveira Vigier, S. Royer and F. Jérôme, *Chem. Soc. Rev.*, 2012, **41**, 7108.
3 E. L. Smith, A. P. Abbott and K. S. Ryder, *Chem. Rev.*, 2014, **114**, 11060–11082.
4 B. Gurkan, H. Squire and E. Pentzer, *J. Phys. Chem. Lett.*, 2019, **10**, 7956–7964.
5 B. B. Hansen, S. Spittle, B. Chen, D. Poe, Y. Zhang, J. M. Klein, A. Horton, L. Adhikari, T. Zelovich, B. W. Doherty, B. Gurkan, E. J. Maginn, A. Ragauskas, M. Dadmun, T. A. Zawodzinski, G. A. Baker, M. E. Tuckerman, R. F. Savinell and J. R. Sangoro, *Chem. Rev.*, 2021, **121**, 1232.
6 D. Yu, Z. Xue and T. Mu, *Chem. Soc. Rev.*, 2021, **50**, 8596.
7 M. A. R. Martins, S. P. Pinho and J. A. P. Coutinho, *J. Solution Chem.*, 2019, **48**, 962.
8 D. O. Abranches and J. A. P. Coutinho, *Annu. Rev. Chem. Biomol. Eng.*, 2023, **14**, 141.
9 C. Russ and B. König, *Green Chem.*, 2012, **14**, 2969.
10 M. Francisco, A. van den Bruinhorst and M. C. Kroon, *Angew. Chem., Int. Ed.*, 2013, **52**, 3074.
11 G. Di Carmine, A. P. Abbott and C. D'Agostino, *React. Chem. Eng.*, 2021, **6**, 582.
12 L. Duan, L.-L. Dou, L. Guo, P. Li and E.-H. Liu, *ACS Sustainable Chem. Eng.*, 2016, **4**, 2405.
13 F. Oyoun, A. Toncheva, L. C. Henríquez, R. Grougnet, F. Laoutid, N. Mignet, K. Alhareth and Y. Corvis, *ChemSusChem*, 2023, **16**, e202300669.
14 D. Yu, D. Jiang, Z. Xue and T. Mu, *Green Chem.*, 2024, **26**, 7478.
15 R. E. Morris, *Chem. Commun.*, 2009, 2990.
16 B. Zhang, J. Zhang and B. Han, *Chem. – Asian J.*, 2016, **11**, 2610.
17 P. Li, F.-F. Cheng, W.-W. Xiong and Q. Zhang, *Inorg. Chem. Front.*, 2018, **5**, 2693.
18 R. A. Maia, B. Louis and S. A. Baudron, *CrystEngComm*, 2021, **23**, 5016.
19 N. Stock and S. Biswas, *Chem. Rev.*, 2012, **112**, 933.
20 J. Ren, X. Dyosiban, N. Musyoka, H. W. Langmi, M. Mathe and S. Liao, *Coord. Chem. Rev.*, 2017, **352**, 187.
21 S. Kumar, S. Jain, M. Nehra, N. Dilbaghi, G. Marrazza and K.-H. Kim, *Coord. Chem. Rev.*, 2020, **420**, 213407.
22 K. Pobłocki, J. Drzeżdżon, B. Gawdzik and D. Jacewicz, *Green Chem.*, 2022, **24**, 9402.
23 E. R. Parnham, E. A. Drylie, P. S. Wheatley, A. M. Z. Slawin and R. E. Morris, *Angew. Chem., Int. Ed.*, 2006, **45**, 4962.
24 J. Zhang, T. Wu, S. Chen, P. Feng and X. Bu, *Angew. Chem., Int. Ed.*, 2009, **48**, 3486.
25 E. A. Drylie, D. S. Wragg, E. R. Parnham, P. S. Wheatley, A. M. Z. Slawin, J. E. Warren and R. E. Morris, *Angew. Chem., Int. Ed.*, 2007, **46**, 7839.
26 R. A. Maia, B. Louis and S. A. Baudron, *Dalton Trans.*, 2021, **50**, 4145.
27 M. Teixeira, R. A. Maia, S. Shanmugam, B. Louis and S. A. Baudron, *Microporous Mesoporous Mater.*, 2022, **343**, 112148.
28 M. Teixeira, R. A. Maia, L. Karmazin, B. Louis and S. A. Baudron, *CrystEngComm*, 2022, **24**, 601.
29 Y. Zang, L.-K. Li and S.-Q. Zang, *Coord. Chem. Rev.*, 2021, **440**, 213955.

30 S. Xian, Y. Lin, H. Wang and J. Li, *Small*, 2021, **17**, 2005165.
31 C. Volkringer, J. Marrot, G. Férey and T. Loiseau, *Cryst. Growth Des.*, 2008, **8**, 685.
32 D. J. Levine, M. I. Gonzalez, C. M. Legendre, T. Runčeski, J. Oktawiec, K. A. Colwell and J. R. Long, *ChemMedChem*, 2017, **17**, 1739.
33 J. Sun, T. Huang, Q. Yin, L. Li, T.-F. Liu, X.-S. Huang and R. Cao, *Cryst. Growth Des.*, 2020, **20**, 8021.
34 B. Darkhijav, Q.-L. Suo, Y.-Y. Gao, E.-H. Hai, R.-J. Xie, N. Zhu and L.-M. Han, *Chin. J. Struct. Chem.*, 2014, **33**, 585.
35 A. Kobayashi, H. Hara, T. Yonemura, H.-C. Chang and M. Kato, *Dalton Trans.*, 2012, **42**, 1878.
36 C. Hua and T. U. Connell, *Aust. J. Chem.*, 2023, **76**, 686.
37 F. Hu, Z. Di, M. Wu and J. Li, *Dalton Trans.*, 2020, **49**, 8836.
38 M. Almàši, V. Zeleňák, R. Gyepes, L. Zauška and S. Bourrelly, *RSC Adv.*, 2020, **13**, 32323.
39 T. Devic, P. Horcajada, C. Serre, F. Salles, G. Maurin, B. Moulin, D. Heurtaux, G. Clet, A. Vimont, J.-M. Grenèche, B. Le Ouay, F. Moreau, E. Magnier, Y. Filinchuk, J. Marrot, J.-C. Lavalley, M. Daturi and G. Férey, *J. Am. Chem. Soc.*, 2010, **132**, 1127.
40 Y. Sun, Y. Sun, H. Zheng, H. Wang, Y. Han, Y. Yang and L. Wang, *CrystEngComm*, 2016, **18**, 8664.
41 D. S. Raja, J.-H. Luo, C.-T. Yeh, Y.-C. Jiang, K.-F. Hsu and C.-H. Lin, *CrystEngComm*, 2014, **16**, 1985.
42 S. Bhattacharjee, T. Chakraborty, S. Banerjee, A. K. Das and A. Bhaumik, *Dalton Trans.*, 2024, **53**, 11120.
43 S. P. Simeonov and C. A. M. Afonso, *RSC Adv.*, 2016, **6**, 5485.
44 J. Yang, C. Trickett, S. Alahmadi, A. Alshammari and O. M. Yaghi, *J. Am. Chem. Soc.*, 2017, **139**, 8118.
45 S. Rojas, A. Rodríguez-Diéguez and P. Horcajada, *ACS Appl. Mater. Interfaces*, 2022, **14**, 16983.
46 X. Zhang, Z. Chen, X. Liu, S. L. Hanna, X. Wang, R. Taheri-Ledari, A. Maleki, P. Li and O. K. Farha, *Chem. Soc. Rev.*, 2020, **49**, 7406.
47 M. Teixeira and S. A. Baudron, *CrystEngComm*, 2024, **26**, 5978.
48 R. A. Maia, A. Fluck, C. Maxim, B. Louis and S. A. Baudron, *Green Chem.*, 2023, **25**, 9103.
49 *M86-EXX278V1 APEX4 User Manual*, Bruker Corporation, 2021.
50 G. M. Sheldrick, *Acta Crystallogr., Sect. A*, 2015, **71**, 3.
51 G. M. Sheldrick, *Acta Crystallogr., Sect. C*, 2015, **71**, 3.
52 *CrysAlisPro Software System, Version 1.171.43.70a*, Rigaku Oxford Diffraction, 2023.